journal of the mechanical behavior of biomedical materials 151 (2024) 106366

Contents lists available at ScienceDirect

Journal of the Mechanical Behavior of Biomedical Materials

journal homepage: www.elsevier.com/locate/jmbbm

Preparation and characterizations of antibacterial iodine-containing coatings on pure Ti

Qiang Li [a,b,*], Shuaishuai Li [a], Hao Sun [a], Mitsuo Niinomi [a,c,d], Takayoshi Nakano [d]

[a] School of Mechanical Engineering, University of Shanghai for Science and Technology, Shanghai, 200093, PR China
[b] Shanghai Engineering Research Center of High-Performance Medical Device Materials, Shanghai, 200093, PR China
[c] Institute for Materials Research, Tohoku University, 2–1–1, Katahira, Aoba-ku, Sendai 980–8577, Japan
[d] Division of Materials and Manufacturing Science, Graduate School of Engineering, Osaka University, 2–1, Yamada-Oka, Suita, Osaka 565–0871, Japan

ARTICLE INFO

Keywords:
Electrochemical deposition
Coating
Povidone-iodine
Antibacterial properties
Cytotoxicity

ABSTRACT

Iodine-containing coatings were prepared on pure Ti surfaces via electrochemical deposition to enhance their antibacterial properties. The factors influencing iodine content were analyzed using an orthogonal experiment. The electrochemically deposited samples were characterized using scanning electron microscopy with energy dispersive spectroscopy and X-ray photoelectron spectroscopy, and their antibacterial properties and cytotoxicity were evaluated. The results showed that changing the deposition time is an effective way to control the iodine content. The iodine content, coating thickness, and adhesion of the samples increased with deposition time. Iodine in the coatings mainly exists in three forms, which are I_2, I_3^-, and pentavalent iodine. For samples with iodine-containing coatings, the antibacterial ratios against *E. coli* and *S. aureus* were greater than 90% and increased with increasing iodine content. Although the samples with iodine-containing coatings showed some inhibition of the proliferation of MC3T3-E1 cells, the cell viabilities were all higher than 80%, suggesting that iodine-containing coatings are biosafe.

1. Introduction

Ti and its alloys are widely used as hard-tissue substitute materials for artificial bones, joints, and dental implants because of their excellent biocompatibility and mechanical properties (Arrés et al., 2020; Zhang et al., 2019). However, these materials lack antibacterial properties. When Ti implants are placed in a microbial environment, bacteria easily adhere to their surfaces, leading to implant-related infections (IRIs) (Hetrick and Schoenfisch, 2006). Serious IRIs usually require implant removal, which not only causes economic losses to patients but also increases patient mortality (Ong et al., 2009). It has been reported that 1%–2% of total hip joint replacement patients suffer from deep infections (Vielgut et al., 2015). In some retrospective studies, the infection rate of external fixator surgery was approximately 2%–30% (De Bastiani et al., 1984; Neoh et al., 2012). Therefore, it is crucial to improve the antibacterial properties of implants.

Several antibacterial agents have been used to load implant surfaces and enhance their antibacterial properties (Chouirfa et al., 2019). Antibiotics are widely known for their efficient bactericidal effects; however, the frequent use of high-dose antibiotics has accelerated the emergence of antibiotic-resistant strains (Ryan et al., 2019). Antibacterial peptides can significantly reduce bacterial adhesion and biofilm formation in Streptococcus; however, the costly synthesis of peptides limits their widespread application (Gruenheid and Le Moual, 2012). A gradual release of inorganic antibacterial metallic elements such as Ag, Cu, and Zn into the tissues around implants can cause bacterial cell membrane oxidation, resulting in cell death; however, it can have toxic effects on human cells (Gaetke and Chow, 2003; Klasen, 2000; Valko et al., 2005). Iodine is an essential element in the human body, especially for synthesizing thyroid hormones (Braverman, 1994). Compared to other antibacterial agents, iodine-based antiseptics have been widely used in the medical field because of their broad spectrum, high efficiency, and low allergic reactions (Fleischer and Reimer, 2009; Wolcott et al., 2020). Povidone-iodine (PVP–I), a complex of polyvinylpyrrolidone (PVP) and iodine, is the most widely used iodine-based antiseptic. It contains approximately 14% iodine in weight ratio (Hiratsuka et al., 2002), shows bactericidal and antibacterial effects on various viruses, fungi, bacteria, and bacterial spores (Li et al., 2017; Reimer et al., 2002), and is commonly used in clinical practice for disinfection during surgeries, as well as for debriding various traumas

* Corresponding author. School of Mechanical Engineering, University of Shanghai for Science and Technology, Shanghai, 200093, PR China
E-mail addresses: jxli@tju.edu.cn, liqiang@usst.edu.cn (Q. Li).

https://doi.org/10.1016/j.jmbbm.2023.106366
Received 28 November 2023; Received in revised form 28 December 2023; Accepted 31 December 2023
Available online 1 January 2024

(Eggers, 2019). PVP-I was impregnated into the anodic oxide of an Al disk specimen, resulting in an improved friction resistance (Hiratsuka et al., 2002). Ti and its alloys loaded with iodine exhibit strong antibacterial properties (Shirai et al., 2011; Tsuchiya et al., 2012; Ueoka et al., 2020). Postoperative infections are prevented using iodine-loaded implants, which hardly show significant cytotoxicity (Gillam et al., 2021; Shirai et al., 2014). However, the characterization and formation mechanisms of iodine-containing coatings remain incomplete, and a method for controlling the iodine content in the coatings is required.

Among surface modifications, such as magnetron sputtering (Tverdokhlebov et al., 2012), plasma electrolytic oxidation (He et al., 2023; Qin et al., 2022), hydrothermal methods (Xie et al., 2022), and electrochemical deposition (Agbe et al., 2021), electrochemical deposition is an effective method for preparing iodine-containing coatings because it has the advantages of easy control over the coating composition, low fabrication cost, high processing speed, and high coating purity (Horandghadim et al., 2022). In this study, electrochemical deposition was used to prepare iodine-containing coatings on pure Ti surfaces. The effects of the PVP-I concentration, deposition time, and temperature on the iodine content of the samples were studied through an orthogonal experiment. Samples with iodine-containing coatings were characterized, and their antibacterial performance and cytotoxicity were evaluated.

2. Experiments

2.1. Orthogonal experiment

Ti plates (purity of 99.5%; ZhongNuo Advanced Material (Beijing) Technology Co., Ltd., China) were polished with sandpaper, ultrasonically cleaned, etched in a mixture of hydrofluoric and nitric acids with an HF: HNO_3: H_2O volume ratio of 1:3:10 for 30 s, ultrasonically cleaned again, and finally dried in air.

A fixed voltage of 200 V was used for the electrochemical deposition. When the voltage was lower, the anodization of Ti was the main reaction, and iodine deposition rarely occurred. When the voltage was higher, the Ti plate was severely corroded by the iodine, which also resulted in limited iodine deposition. Electrochemical deposition was performed using a two-electrode system (HSPY-200-02; Beijing Han Sheng Pu Yuan Technology Co., Ltd., China) with a Ti plate as the anode and a Pt plate as the cathode. A beaker containing the electrolyte was placed in a water bath at a fixed temperature. The effects of three deposition parameters—PVP-I (Shanghai Aladdin Biochemical Technology Co., Ltd., China) concentration, deposition time, and temperature—were studied using an orthogonal experiment. The factor levels used in the orthogonal experiments are listed in Table 1. An L9 (3^3) orthogonal experimental table (Table 2) was constructed using three factors and three levels. The iodine-containing coatings were prepared by electrochemical deposition following the aforementioned steps according to the three fixed factors listed in Table 2. The iodine content of the prepared sample was used as the evaluation index. The influence of the three deposition parameters on the iodine content of the samples was determined.

Table 1
Factor levels of orthogonal experiment.

Level	Factors		
	PVP-I concentration /mass%	Deposition time /s	Deposition temperature /°C
1	0.2	60	30
2	0.3	150	40
3	0.4	240	50

Table 2
Orthogonal experiment results and range analysis of iodine content.

Process NO.	Factors			Results
	PVP-I concentration /mass%	Deposition time /s	Deposition temperature /°C	Iodine content /mass%
NO. 1	0.2	60	30	1.71
NO. 2	0.2	150	40	2.24
NO. 3	0.2	240	50	3.70
NO. 4	0.3	60	40	2.89
NO. 5	0.3	150	50	2.44
NO. 6	0.3	240	30	2.87
NO. 7	0.4	60	50	2.84
NO. 8	0.4	150	30	3.39
NO. 9	0.4	240	40	4.53

2.2. Surface characterization

The surface morphologies of the samples were observed using scanning electron microscopy (SEM; FEI Quanta 450FEG, USA) at an accelerating voltage of 30 kV, and the surface chemical compositions were analyzed using energy dispersive spectroscopy (EDS). The chemical states of the main elements were analyzed by an X-ray photoelectron spectroscopy (XPS; AIXS Ultra DLD, Japan) with a monochromatic Al Kα ($h\nu = 1486.6$ eV) X-ray radiation source. The iodine concentration in the solution was determined using inductively coupled plasma mass spectrometry (ICP-MS; PE-NexION, 2000, USA).

2.3. Adhesion test

The bonding strength between the coating and the substrate was measured using an automatic scratching tester (WS-2005; Lanzhou Zhongke Kaihua Technology Development Co., Ltd., China) with a diamond indenter having an apex angle of 120° and a tip radius of 0.2 mm. The scratching test was performed under progressive loading conditions. The normal load was increased from 0 to 40 N at a loading rate of 40 N/min, and the acoustic signal and friction were recorded. The bonding strength was evaluated by determining the critical load of the coating that failed on the substrate.

2.4. Antibacterial test

The antibacterial properties of the prepared samples were evaluated using *S. aureus* ATCC 29213 (Guangdong Microbial Culture Collection Center, China) and *E. coli* ATCC 25922 (Guangdong Microbial Culture Collection Center, China) as test strains. The number of colonies was determined by the plate-counting method. The samples were subjected to antibacterial tests, using Ti as a control. All samples were immersed in an alcohol solution for 0.5 h and then placed in a 24-well plate. The bacterial solution was diluted to 10^6 CFU/mL with Luria-Bertani liquid medium, and then 0.2 mL of the diluted bacterial solution was added to each sample surface. Sterile normal saline was added to the empty wells to prevent the evaporation of water from the bacterial solution. The 24-well plates were placed in a constant temperature incubator at 37 °C for 18 h. The co-culture solution was diluted 10^6 times with the sterile phosphate-buffered saline solution, and 100 μL of the diluent was obtained using a pipette gun and evenly coated on the solid medium in a Petri dish with a diameter of 90 mm. After incubation at 37 °C in a constant-temperature incubator for 18 h, the number of colonies in each Petri dish was recorded.

2.5. Cytocompatibility test

Mouse preosteoblast cells (MC3T3-E1; iCell Bioscience Inc., China) were used to evaluate the cytotoxicity of the samples. The culture medium was α-MEM supplemented with 10% fetal bovine serum. First, the

samples were sterilized at 121 °C for 1200 s. Because they were solid flakes, extraction was conducted at 37 °C for 24 h at a liquid volume ratio of 1.25 cm^2/mL according to the ISO10993-12 standard. Each sample extract (100 μL) was placed into separate 96-well plates. Three parallel wells were used for each sample. MC3T3-E1 cells were then inoculated into each well at a density of 2×10^3 cells/well for 24 h, and 1×10^3 cells/mL for 96 and 168 h of culture. As a control, MC3T3-E1 cells were seeded directly onto the bottom of the wells without extract. The 96-well plates were placed in a humidified incubator with a 5% CO_2 atmosphere for 24, 96, and 168 h at 37 °C. After culturing, each well was rinsed three times with PBS. The culture medium (100 μL) with 10% MTT assay was added to each well and then incubated in a humidified incubator at 37 °C with a 5% CO_2 atmosphere for an additional 4 h. The supernatant was aspirated, and 100 μL of dimethyl sulfoxide (DMSO) was added to each well followed by gentle shaking for 600 s. Optical density (OD) was measured at a wavelength of 570 nm using a TECAN SPARK 10M enzyme-labeled instrument.

3. Results and discussion

3.1. Orthogonal experiment results

The mass fractions of iodine in the samples prepared according to the orthogonal experiment were measured using EDS, as listed in Table 2. Intuitive analysis methods were used to determine the order of influence of these factors. As shown in Table 3, K_1, K_2, and K_3 represent the average values of the iodine contents corresponding to the first, second, and third levels of each factor, respectively (Qin et al., 2023). The maximum difference (Range R_K) between K_1, K_2, and K_3 reflects the overall effect of the factor. The greater the range value of a factor, the greater its influence on the results (Wang et al., 2020). The range analysis results suggest that the deposition time had the greatest influence on the iodine content, with the highest range of 1.22. The deposition temperature had the lowest value of 0.56, indicating the lowest impact. Based on the factor levels listed in Table 1 and the range analysis results, changing the deposition time is the most effective method for adjusting the iodine content. Therefore, iodine-containing coatings were prepared in 0.2% PVP-I solution at 30 °C for 60, 150, and 240 s in a subsequent study.

3.2. Characterizations of coating

The surface morphologies of the Ti plates before and after electrochemical deposition are shown in Fig. 1. Scratches were observed on the surface of the Ti plate before electrochemical deposition, as shown in Fig. 1a. The coating with a thickness of approximately 0.16 μm was obtained on the surface after electrochemical deposition for 60 s, and the scratches were completely covered (Fig. 1b). With an increase of deposition time, a minimal change in surface morphology was observed (Fig. 1c and d); however, the thickness of the coating gradually increased to 0.26 and 0.36 μm after electrochemical deposition for 150 and 240 s, respectively.

The chemical compositions of the samples after electrochemical deposition are listed in Table 4. Ti, O, and I were detected using EDS. As the deposition time increased, the iodine content increased with decreasing Ti content, indicating that iodine was continuously deposited on the surface of the sample. The presence of O was due to the formation of Ti–O and I–O compounds (Gai et al., 2021), which were further studied via XPS. The elemental distribution of the sample after 60 s of deposition is shown in Fig. 2. Ti, O, and I were uniformly distributed on the surface of the sample, and minimal elemental aggregation was observed.

Table 3
Range analysis of iodine content (mass%).

Calculated value	Factors		
	PVP-I concentration	Deposition time	Deposition temperature
K_1	2.55	2.48	2.66
K_2	2.73	2.69	3.22
K_3	3.59	3.70	2.99
Range R_K	1.04	1.22	0.56

The full XPS spectrum (Fig. 3a) suggested the presence of Ti, O, I, F, C, and N in the sample after electrochemical deposition for 60 s. The appearance of C and N is mainly due to air pollution (Wu et al., 2014), and the presence of F is attributed to electrolyte residues after etching.

For the XPS spectrum of Ti2p (Fig. 3b), the two peaks at 458.5 and 464.2 eV corresponded to Ti2p3/2 and Ti2p1/2, respectively. High-resolution spectral analysis revealed the characteristic binding energy peaks of TiO_2 (Gai et al., 2021). At the beginning of deposition, Ti was quickly oxidized to Ti^{4+} (Eq. (1)), followed by the formation of a TiO_2 film according to Eq. (2) (Sulka et al., 2013).

$$Ti - 4e^- \rightarrow Ti^{4+} \quad \text{Eq. 1}$$

$$Ti^{4+} + 2H_2O \leftrightarrows TiO_2 + 4H^+ \quad \text{Eq. 2}$$

Six peaks were fitted to the XPS spectrum of I3d (Fig. 3c), suggesting complex reactions of PVP-I during the electrochemical deposition process. The peaks at 623.4, 620.4, and 618.5 eV corresponded to I3d5/2, and the peaks at 635.4, 631.8, and 629.9 eV corresponded to I3d3/2.

The peaks at 620.4 and 631.8 eV were attributed to I_2 (Morizet et al., 2021). I^- generated by the dissociation of PVP-I in the solution (Eqs. (3) and (4)) (Sa et al., 2017), and I_2 formed at the anode by an oxidation reaction (Eq. (5)).

$$PVP\text{-}I_2 \rightarrow PVP\text{-}I^+I^- \quad \text{Eq. 3}$$

$$PVP\text{-}I^+I^- \rightarrow PVP\text{-}I^+ + I^- \quad \text{Eq. 4}$$

$$2I^- - 2e^- \rightarrow I_2 \quad \text{Eq. 5}$$

The peaks at 618.5 and 629.9 eV were attributed to I_3^-, which was generated from $PVP\text{-}I^+I^-$ (Eq. (6)) and the chemical equilibrium between I_2 and I^- (Eq. (7)) (Sa et al., 2017; Shih et al., 2018).

$$2PVP\text{-}I^+I^- \leftrightarrows (PVP)_2I^+ + I_3^- \quad \text{Eq. 6}$$

$$I_2 + I^- \leftrightarrows I_3^- \quad \text{Eq. 7}$$

The peaks at 623.4 and 635.4 eV belonged to pentavalent iodine (Yamaguchi et al., 2021). Because I_2 was unstable, disproportionation occurred in the solution (Eqs. (8) and (9)) (Gottardi, 1999). Pentavalent iodine mainly existed in the form of HIO_3 or I_2O_5 in the coating (Bagwasi et al., 2012).

$$I_2 + H_2O \leftrightarrows HOI + H^+ + I^- \quad \text{Eq. 8}$$

$$3HOI \leftrightarrows IO_3^- + 2I^- + 3H^+ \quad \text{Eq. 9}$$

In the O1s XPS spectra (Fig. 3d), the peak at 529.6 eV belonged to the TiO_2 lattice O, and the peak at 531 eV is attributed to chemically adsorbed O (Bao et al., 2021).

3.3. Deposition process analysis

The current intensity during deposition was recorded, as shown in Fig. 4. The electrochemical deposition process can be divided into three stages according to the change in current intensity. The first stage corresponds to the deposition from the start to approximately 5 s. Initially, the oxidation of Ti (Eq. (1)) occurred rapidly, and a dense TiO_2 film formed on the Ti surface (Eq. (2)), resulting in a sharp decrease in the current density. The second stage was the deposition time, which ranged from 5 to 200 s. The gradual decrease in the current density was mainly due to the deposition of iodine on the substrate. The I^- from PVP-I (Eqs. (3) and (4)) are oxidized to I_2 at the anode (Eq. (5)). An iodine-

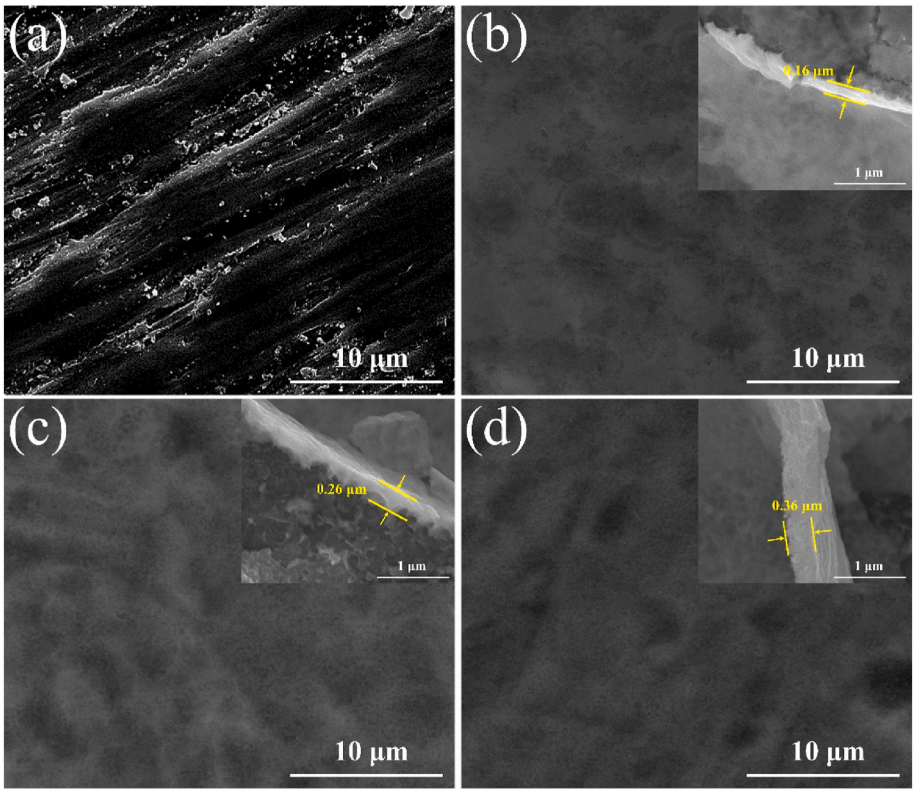

Fig. 1. SEM morphologies of (a) Ti and the samples after electrochemical deposition in a 0.2% PVP-I solution at 30 °C for (b) 60 s, (c) 150 s, and (d) 240 s.

Table 4
Chemical compositions of the samples after electrochemical deposition.

Deposition time /s	Ti /mass%	O /mass%	I /mass%
60	91.15	7.14	1.71
150	90.05	7.75	2.20
240	86.72	10.07	3.21

containing coating formed and gradually covered the surface of the sample. The conductivity of the anode decreased, resulting in a decrease in current intensity. When the deposition time exceeded 200 s, the electrochemical deposition entered the third stage, at which the current density changed slightly. The electrochemical reaction proceeded continuously and the coating became thicker.

The reactions involved in electrochemical deposition are shown in Fig. 4. The reactions of Eqs. (1) and (2) show the anodization process of the substrate. I^- was continuously provided by PVP-I according to the reactions of Eqs. (3) and (4) and consumed by the electrode reaction in Eq. (5) to generate I_2 on the substrate. The reaction of Eqs. (6)–(9) represent the chemical equilibria of iodine surrounding the substrate. I_3^- and pentavalent iodine showed weak peaks in the XPS spectrum (Fig. 3c), and their contents were limited in the sample.

3.4. Adhesion

The friction force and acoustic signal curves of the iodine-containing coatings deposited at various times are shown in Fig. 5. The acoustic signal was hardly detected because the iodine-containing coatings prepared by electrochemical deposition using the PVP-I solution were soft. The critical load of iodine-containing coatings can be determined from the friction curve to evaluate the bonding strength between the coating and substrate (Pelletier et al., 2011). At the beginning of the test, the indenter touched the coating, and the friction increased linearly with increasing load. When the applied load exceeded a critical force, the coating was destroyed and the indenter began to scratch the substrate, increasing the slope of the friction curves. By fitting the friction curve, the intersection point of the two lines was considered the critical load, which reflected the adhesion of the coating. For the samples subjected to electrochemical deposition for 60, 150, and 240 s, the critical loads were 11.6, 18.1, and 24.4 N, respectively. As the deposition time increased, the critical load gradually increased, suggesting an increase in the adhesion of the coating.

3.5. Antibacterial activities

The *E. coli* and *S. aureus* colonies in the samples are shown in Fig. 6. A large number of *E. coli* and *S. aureus* colonies were observed on the Ti agar plate, which was used as the blank control in this study. The colonies of *E. coli* and *S. aureus* in the Petri dishes containing samples with iodine-containing coatings were significantly reduced. The antibacterial ratio for each sample was calculated using the following equation:

$$\text{Antibacterial ratio } (\%) = (A - B)/A \times 100\% \quad \text{Eq. 10}$$

where, A and B are the colony numbers of the blank control and test samples, respectively.

After electrochemical deposition for 60 s, the antibacterial ratios of the samples against *E. coli* and *S. aureus* were 93.2% and 96.3%, respectively. As the deposition time was increased to 150 s, the antibacterial ratios of the samples against *E. coli* and *S. aureus* increased to 96.2% and 97.9%, respectively. At a deposition time of 240 s, *E. coli* and *S. aureus* colonies were barely observed, indicating that the antimicrobial ratios were higher than 99%.

As the deposition time increased, the iodine content of the samples increased. For the samples after electrodeposition for 60, 150, and 240 s, the iodine concentrations in the 18 h co-culture solution were 1.8, 2.4, and 3.5 ppm, respectively, showing an increasing trend. As indicated by the XPS spectrum, there were three states of iodine in the coatings,

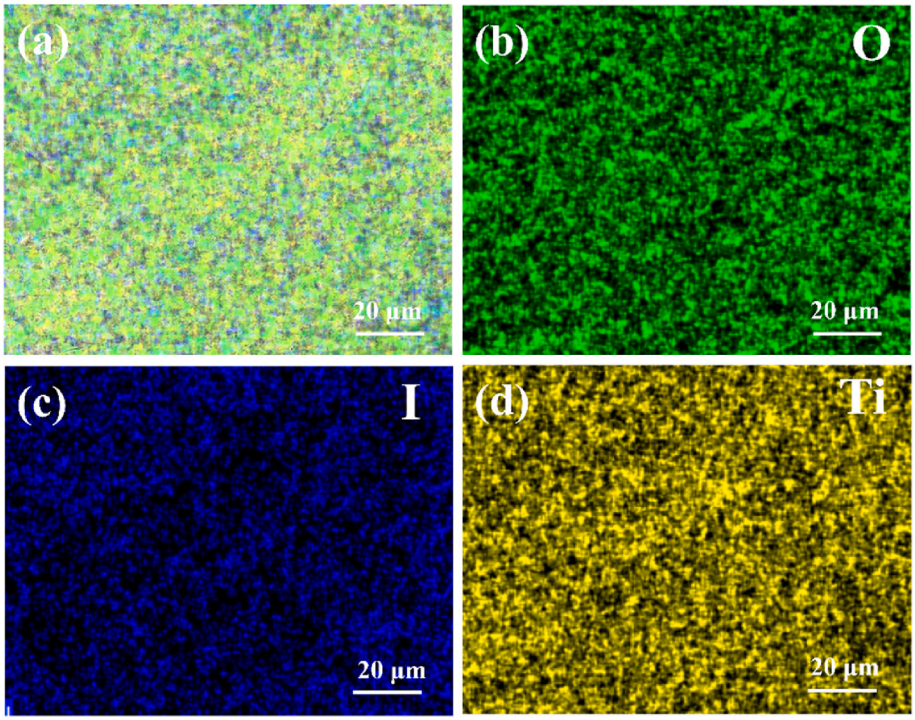

Fig. 2. (a) EDS layered image of the sample after 60 s electrochemical deposition and the corresponding element distributions of (b) O, (c) I, and (d) Ti.

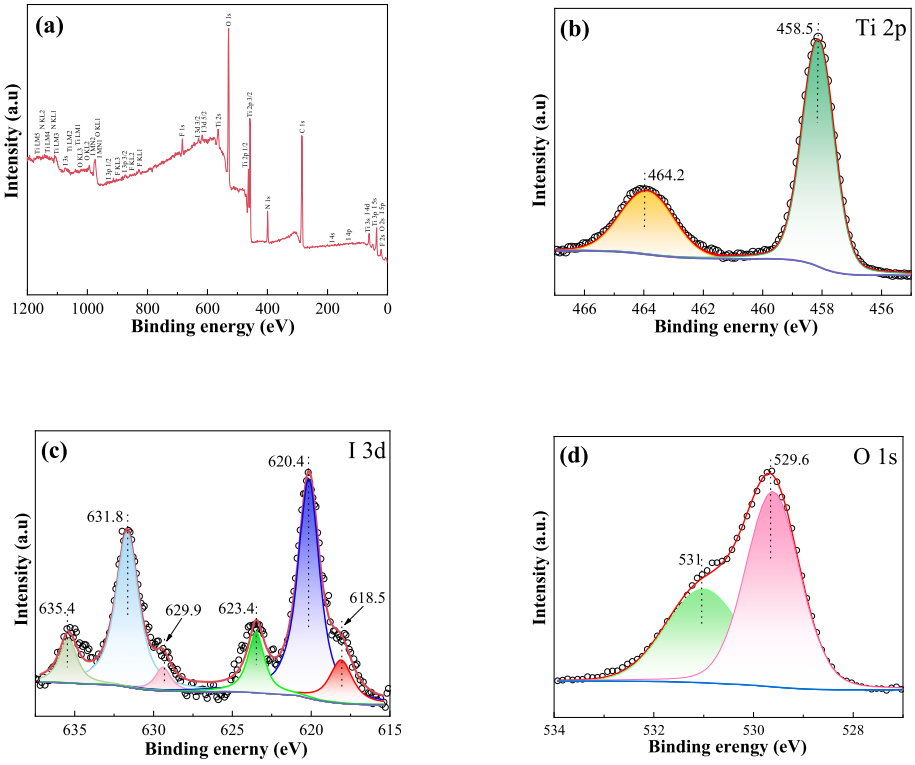

Fig. 3. (a) XPS survey spectra of the sample after 60 s electrochemical deposition and the high-resolution spectra of (b) Ti, (c) I, and (d) O.

which were I_2, I_3^-, and pentavalent iodine. Although only I_2 has the effect of inhibiting bacterial reproduction, I_3^- and pentavalent iodine can gradually transform into I_2 because of the chemical instability (Bagwasi et al., 2012; Shih et al., 2018). The released free iodine can pass through the cell membrane, promoting the denaturation of microbial body proteins until coagulation (Gillam et al., 2021; Reimer et al., 2002). It is believed that free iodine can be released from the prepared iodine-containing coating; thus, the samples after electrochemical deposition effectively inhibited the growth of the surrounding bacteria and exhibited good antibacterial activities.

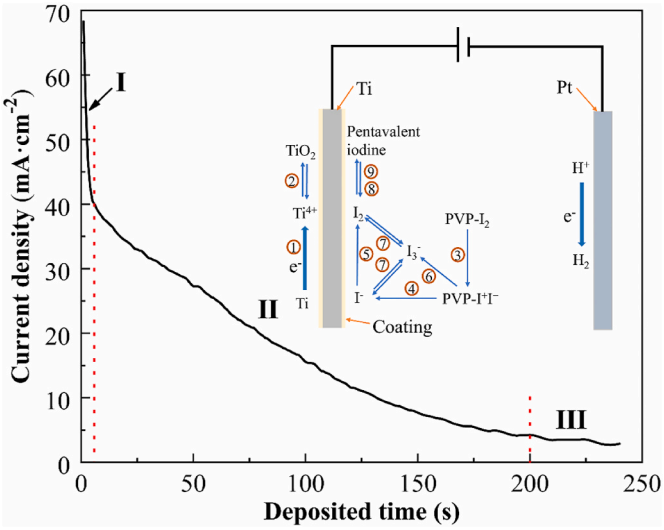

Fig. 4. Change in current density and the reactions in the deposition process.

3.6. Cytotoxicity

The OD values of MC3T3-E1 cells in each group were measured to evaluate cell viability. The cell viability was expressed as a percentage and calculated using the following equation (Fan et al., 2022):

Cell viability (%) was calculated as OD (test) / OD (blank) × 100% Eq. 11

The cell viabilities of the samples after 24, 96, and 168 h of culture are shown in Fig. 7. After 24 h of culture, the cell viability of the electrochemically deposited samples was lower than that of the control. A significant decrease ($P < 0.05$) was observed for the sample deposited for 240 s. Compared to the control, significant decreases were observed in all electrochemically deposited samples after 96 h of culture. Similar phenomena were observed after 168 h of culture. The cell viabilities of the electrochemically deposited samples were lower than 100%. These results suggest that iodine has an inhibitory effect on the proliferation of MC3T3-E1 cells, similar to the results of Durani and Leaper (2008). Freeman pointed out that for non-cytotoxic or irritating effects, the highest concentration of I_2 from PVP-I was approximately 25 ppm (Freeman et al., 2022). After electrodeposition for 60, 150, and 240 s, the iodine concentrations in the extracts were 1.4, 1.6, and 2.1 ppm, respectively, which were all significantly lower than 25 ppm. Additionally, according to ISO10993-5, the three electrochemically deposited samples are regarded as biosafe because their cell viabilities are all above 80% (Fan et al., 2022).

3.7. Discussion

An iodine-containing coating was electrochemically deposited on an anodized Al surface by Hashimoto et al., in 1999 (Hashimoto et al., 1999), and a series of iodine-containing coatings was subsequently applied to the surfaces of Ti and Ti alloys after anodization (Shirai et al., 2011; Tsuchiya et al., 2012). In this study, one-step electrochemical deposition without pre-anodization was carried out on pure Ti at a deposition voltage of 150–200 V. Details including the iodine content, coating thickness, and adhesion were not presented by Hashimoto et al.,

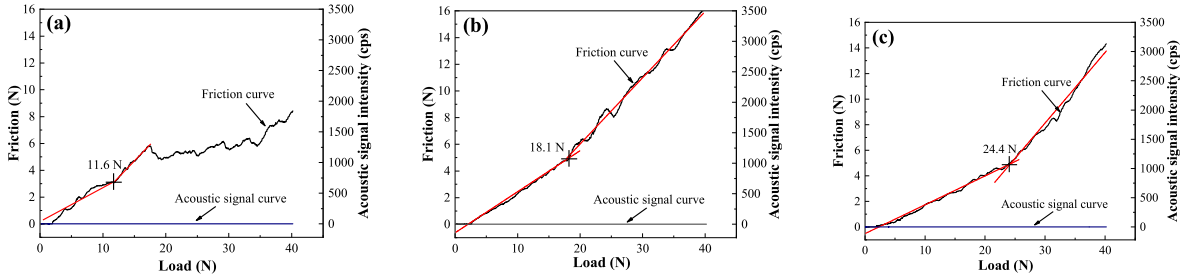

Fig. 5. Friction and acoustic signal curves of the samples after electrochemical deposition for (a) 60 s, (b) 150 s, and (c) 240 s.

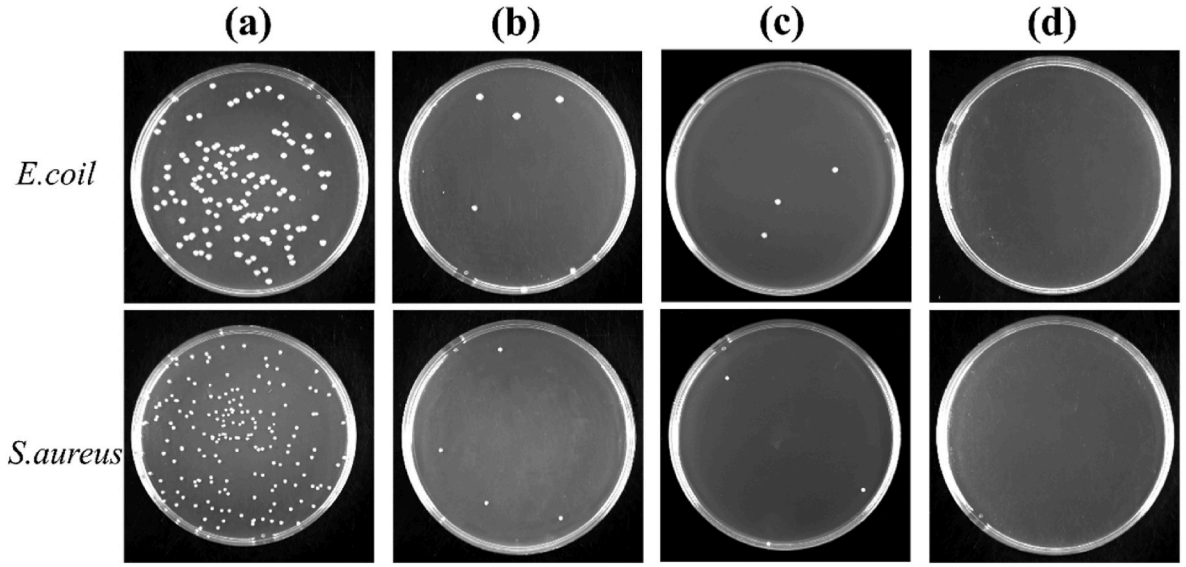

Fig. 6. Colonies of *E. coli* and *S. aureus* of (a) Ti and the samples after electrochemical deposition for (b) 60 s, (c) 150 s, and (d) 240 s.

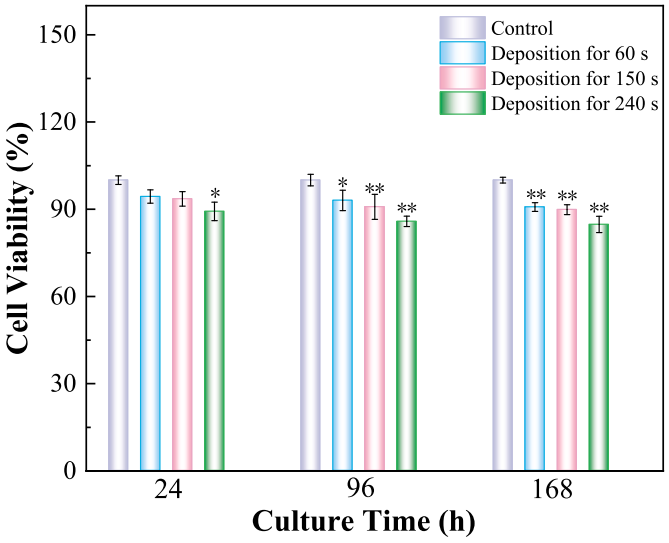

Fig. 7. Viability of MC3T3-E1 cells for the samples after 24, 96, and 168 h culture (*denotes a significant difference at $P < 0.05$ compared to control, **denotes a significant difference at $P < 0.01$ compared to control).

but are provided in this study.

F^- and Cl^- etch TiO_2 according to Eqs. (12) and (13) (Allam and Grimes, 2007; Nguyen et al., 2008). In this study, it was supposed that I^- also etched TiO_2 according to Eq. (14).

$$TiO_2 + 6Cl^- + 4H^+ \rightarrow TiCl_6^{2-} + 2H_2O \quad \text{Eq. 12}$$

$$TiO_2 + 6F^- + 4H^+ \rightarrow TiF_6^{2-} + 2H_2O \quad \text{Eq. 13}$$

$$TiO_2 + 6I^- + 4H^+ \rightarrow TiI_6^{2-} + 2H_2O \quad \text{Eq. 14}$$

With the increase in deposition time, the coating became thicker, and the interaction between the coating and substrate continuously occurred, increasing the adhesion. When deposition time was increased from 60 to 240 s, the critical load increased from 11.6 to 24.4 N. The critical loads of the iodine-containing coatings were higher than those of HAp coatings prepared by electrochemical deposition (2.3–4.3 N) and plasma spray (11.8–16.0 N) (Cotrut et al., 2022; Hussain et al., 2023). Because the critical load reflects the bonding strength between the coating and the substrate, the improved critical load is beneficial to the long-term stability of implants (Ahmad et al., 2023; Cao et al., 2023).

According to the orthogonal experiment, the influence of the deposition parameters on the iodine content followed the order deposition time > PVP-I concentration > deposition temperature. For the three-factor levels, the deposition time, PVP-I concentration, and deposition temperature increased equidistantly in the orthogonal experiment (Table 1). The increase in the deposition time was 90 s, which was 150% of the initial deposition time (60 s). The increase in the PVP-I concentration (0.1%) was 50% of the initial PVP-I concentration (0.2%). However, the increase in the deposition temperature (10 K) was approximately 3.3% of the initial deposition time (303 K) when using the absolute temperature. The variation in the increasing ratio of the parameters significantly affects the order of influence. Additionally, the electrodeposition of iodine-containing coatings is a complex process that mainly involves the generation of I^- from PVP-I, electromigration of I^- in the electrolyte, interaction with the substrate, and electrode reaction (Eq. (5)) of forming I_2. According to the XPS results, iodine was mainly in the form of I_2. As a simple electrode reaction (Eq. (5)), the reaction product accumulated over a prolonged time, and the reaction speed was proportional to I^- concentration, which was mainly determined by PVP-I concentration. With the increase in deposition time, more I^- continuously generated from PVP-I and migrated onto the substrate, and then more I_2 formed according to the electrode reaction, increasing iodine content and coating thickness. The increase in PVP-I concentration leads to an increase in I^- concentration, which accelerates the electrode reaction and then promotes the forming of I_2. Increasing the deposition temperature can also improve the electrical reaction; however, it may decrease the stability of the I-containing coating, resulting in loss of iodine (Satoh and Imai, 2020). Compared with preparing electrolytes with various PVP-I concentrations and changing the deposition temperatures, adjusting the deposition time was more convenient. Moreover, the thickness of the coating and the iodine content of the sample increased with increasing deposition time, leading to an increase in the iodine concentration in the solution and the antibacterial ratio. By changing the deposition time, it is feasible to obtain different iodine contents to balance the antibacterial properties and cytocompatibility.

Compared to the iodine-immobilized metal-organic framework prepared by Teng et al. (2021), the iodine-containing coatings showed higher antibacterial activities. They also exhibited better biosafety than the prepared polyurethane-iodine complexes (Jie et al., 2010), which showed similar antibacterial activities. Therefore, iodine-containing coatings exhibit a desirable balance between antibacterial activity and cytocompatibility. Thus, the developed electrochemical deposition method is feasible for improving the antibacterial activity of implants.

4. Conclusions

The following conclusions were drawn from the above results and discussions.

(1) The PVP-I concentration, deposition time, and deposition temperature affected the iodine content of the electrochemically deposited samples, with the deposition time having the greatest impact. With increasing deposition time, both iodine content and adhesion gradually increased.
(2) Iodine uniformly distributed on the surface of Ti plates, and mainly existed in three forms—I_2, I_3^-, and pentavalent iodine.
(3) Samples with iodine-containing coatings exhibited remarkable antibacterial properties, and the antibacterial ratio increased with increasing iodine content. Although iodine showed some inhibition of cell proliferation, all the electrochemically deposited samples exhibited cell viabilities above 80%, suggesting that they were biosafe.

CRediT authorship contribution statement

Qiang Li: Writing – review & editing, Supervision, Methodology, Funding acquisition, Conceptualization. **Shuaishuai Li:** Writing – review & editing, Validation, Methodology, Conceptualization. **Hao Sun:** Resources, Investigation. **Mitsuo Niinomi:** Investigation. **Takayoshi Nakano:** Investigation.

Declaration of competing interest

The authors declare that they have no known competing financial interests or personal relationships that could have appeared to influence the work reported in this paper.

Data availability

Data will be made available on request.

Acknowledgements

This work was partially supported by the Shanghai Engineering Research Center of High-Performance Medical Device Materials (No. 20DZ2255500).

References

Agbe, H., Sarkar, D.K., Chen, X.G., 2021. Electrochemically synthesized silver phosphate coating on anodized aluminum with superior antibacterial properties. Surf. Coating. Technol. 428, 127892.

Ahmad, K., Batool, S.A., Farooq, M.T., Minhas, B., Manzur, J., Yasir, M., Wadood, A., Avcu, E., Ur Rehman, M.A., 2023. Corrosion, surface, and tribological behavior of electrophoretically deposited polyether ether ketone coatings on 316L stainless steel for orthopedic applications. J. Mech. Behav. Biomed. 148, 106188.

Allam, N.K., Grimes, C.A., 2007. Formation of vertically oriented TiO2 nanotube arrays using a fluoride free HCl aqueous electrolyte. J. Phys. Chem. C 111, 13028–13032.

Arrés, M., Salama, M., Rechena, D., Paradiso, P., Reis, L., Alves, M.M., Botelho do Rego, A.M., Carmezim, M.J., Vaz, M.F., Deus, A.M., Santos, C., 2020. Surface and mechanical properties of a nanostructured citrate hydroxyapatite coating on pure titanium. J. Mech. Behav. Biomed. 108, 103794.

Bagwasi, S., Tian, B., Chen, F., Zhang, J., 2012. Synthesis, characterization and application of iodine modified titanium dioxide in phototcatalytical reactions under visible light irradiation. Appl. Surf. Sci. 258, 3927–3935.

Bao, Y., Wang, W., Cui, W., Qin, G., 2021. Corrosion resistance and antibacterial activity of Ti-N-O coatings deposited on dental titanium alloy. Surf. Coating. Technol. 419, 127296.

Braverman, L.E., 1994. Iodine and the thyroid: 33 years of study. Thyroid 4, 351–356.

Cao, H., Tian, P., Deng, J., Li, Y., Wang, C., Han, S., Zhao, X., 2023. Electrochemical deposition multi-walled carbon nanotube coatings on the surface of Ti6Al4V alloy for enhancing its biotribological properties. J. Mech. Behav. Biomed. 142, 105825.

Chouirfa, H., Bouloussa, H., Migonney, V., Falentin-Daudré, C., 2019. Review of titanium surface modification techniques and coatings for antibacterial applications. Acta Biomater. 83, 37–54.

Cotrut, C.M., Ungureanu, E., Ionescu, I.C., Zamfir, R.I., Kiss, A.E., Parau, A.C., Vladescu, A., Vranceanu, D.M., Saceleanu, A., 2022. Influence of magnesium content on the physico-chemical properties of hydroxyapatite electrochemically deposited on a nanostructured titanium surface. Coatings 12, 1097.

De Bastiani, G., Aldegheri, R., Renzi Brivio, L., 1984. The treatment of fractures with a dynamic axial fixator. J. Bone Joint Surg. Br. 66 4, 538–545.

Durani, P., Leaper, D., 2008. Povidone-iodine: use in hand disinfection, skin preparation and antiseptic irrigation. Int. Wound J. 5, 376–387.

Eggers, M., 2019. Infectious disease management and control with povidone iodine. Infect. Dis. Ther. 8, 581–593.

Fan, L., Sun, W., Zou, Y., Xu, Q.-q., Zeng, R.-C., Tian, J., 2022. Enhanced corrosion resistance, antibacterial activity and biocompatibility of gentamicin-montmorillonite coating on Mg alloy-in vitro and in vivo studies. J. Mater. Sci. Technol. 111, 167–180.

Fleischer, W., Reimer, K., 2009. Povidone-iodine in antisepsis – state of the art. Dermatology 195, 3–9.

Freeman, C., Duan, E., Kessler, J., 2022. Molecular iodine is not responsible for cytotoxicity in iodophors. J. Hosp. Infect. 122, 194–202.

Gaetke, L.M., Chow, C.K., 2003. Copper toxicity, oxidative stress, and antioxidant nutrients. Toxicology 189, 147–163.

Gai, H., Wang, H., Liu, L., Feng, B., Xiao, M., Tang, Y., Qu, X., Song, H., Huang, T., 2021. Potassium and iodide codoped mesoporous titanium dioxide for enhancing photocatalytic degradation of phenolic compounds. Chem. Phys. Lett. 767, 138367.

Gillam, T.A., Goh, C.K., Ninan, N., Bilimoria, K., Shirazi, H.S., Saboohi, S., Al-Bataineh, S., Whittle, J., Blencowe, A., 2021. Iodine complexed poly (vinyl pyrrolidone) plasma polymers as broad-spectrum antiseptic coatings. Appl. Surf. Sci. 537, 147866.

Gottardi, W., 1999. Iodine and disinfection: theoretical study on mode of action, efficiency, stability, and analytical aspects in the aqueous system. Arch. Pharm. 332, 151–157.

Gruenheid, S., Le Moual, H., 2012. Resistance to antimicrobial peptides in Gram-negative bacteria. FEMS Microbiol. Lett. 330, 81–89.

Hashimoto, K., Takaya, M., Maejima, M., Saruwatari, K., Hirata, M., Toda, Y., Udagawa, S., 1999. Antimicrobial characteristics of anodic oxidation coating of aluminum impregnated with iodine compound. Inorg. Mater. + 6, 457–462.

He, X., Feng, T., Cheng, Y., Hu, P., Le, Z., Liu, Z., Cheng, Y.-l., 2023. Fast formation of a black inner α-Al2O3 layer doped with CuO on Al–Cu–Li alloy by soft sparking PEO process. J. Am. Ceram. Soc. 106, 7019–7042.

Hetrick, E.M., Schoenfisch, M.H., 2006. Reducing implant-related infections: active release strategies. Chem. Soc. Rev. 35, 780–789.

Hiratsuka, K., Asakawa, M., Funakoshi, A., Takaya, M., 2002. Effect of impregnation of iodine complex on friction of anodic oxide of aluminum. Tribol. Lett. 13, 77–80.

Horandghadim, N., Ghazanfar-Ahari, Y., Khalil-Allafi, J., 2022. Multiwalled-carbon nanotubes reinforced hydroxyapatite- tantalum pentoxide nanocomposite coating on Nitinol alloy: antibacterial activity and Electrochemical properties. Surface. Interfac. 29, 101773.

Hussain, S., Shah, Z.A., Sabiruddin, K., Keshri, A.K., 2023. Characterization and tribological behaviour of Indian clam seashell-derived hydroxyapatite coating applied on titanium alloy by plasma spray technique. J. Mech. Behav. Biomed. 137, 105550.

Jie, L., Ying, D., Yuyu, S., 2010. Antimicrobial activity and biocompatibility of polyurethane—iodine complexes. J. Bioact. Compat Polym. 25, 185–206.

Klasen, H.J., 2000. Historical review of the use of silver in the treatment of burns. I. Early uses. Burns 26, 117–130.

Li, Q., Korza, G., Setlow, P., 2017. Killing the spores of Bacillus species by molecular iodine. J. Appl. Microbiol. 122, 54–64.

Morizet, Y., Jolivet, V., Trcera, N., Suzuki-Muresan, T., Hamon, J., 2021. Iodine local environment in high pressure borosilicate glasses: an X-ray photoelectron spectroscopy and X-ray absorption spectroscopy investigation. J. Nucl. Mater. 553, 153050.

Neoh, K.G., Hu, X., Zheng, D., Kang, E.T., 2012. Balancing osteoblast functions and bacterial adhesion on functionalized titanium surfaces. Biomaterials 33, 2813–2822.

Nguyen, Q.A., Bhargava, Y.V., Devine, T.M., 2008. Titania nanotube formation in chloride and bromide containing electrolytes. Electrochem. Commun. 10, 471–475.

Ong, K.L., Kurtz, S.M., Lau, E., Bozic, K.J., Berry, D.J., Parvizi, J., 2009. Prosthetic joint infection risk after total hip arthroplasty in the Medicare population. J. Arthroplasty 24, 105–109.

Pelletier, H., Carradò, A., Faerber, J., Mihailescu, I.N., 2011. Microstructure and mechanical characteristics of hydroxyapatite coatings on Ti/TiN/Si substrates synthesized by pulsed laser deposition. Appl. Phys. A 102, 629–640.

Qin, J., Chen, Y., Chen, C., Zhong, S., Yan, Z., Liu, W., Wang, Y., Lai, X., Zhao, Y., Zhao, R., Zhang, R., 2023. Preparation of HA-containing coating by one-step MAO on titanium alloys through synergistic effect of calcium gluconate and calcium glycerophosphate. Surf. Coating. Technol. 466, 129655.

Qin, J., Shi, X., Li, H., Zhao, R., Li, G., Zhang, S., Ding, L., Cui, X., Zhao, Y., Zhang, R., 2022. Performance and failure process of green recycling solutions for preparing high degradation resistance coating on biomedical magnesium alloys. Green Chem. 24, 8113–8130.

Reimer, K., Wichelhaus, T.A., Schäfer, V., Rudolph, P., Kramer, A., Wutzler, P., Ganzer, D., Fleischer, W., 2002. Antimicrobial effectiveness of povidone-iodine and consequences for new application areas. Dermatology 204 (Suppl. 1), 114–120.

Ryan, E.J., Ryan, A.J., González-Vázquez, A., Philippart, A., Ciraldo, F.E., Hobbs, C., Nicolosi, V., Boccaccini, A.R., Kearney, C.J., O'Brien, F.J., 2019. Collagen scaffolds functionalised with copper-eluting bioactive glass reduce infection and enhance osteogenesis and angiogenesis both in vitro and in vivo. Biomaterials 197, 405–416.

Sa, A., Sawatdee, S., Phadoongsombut, N., Buatong, W., Nakpeng, T., Sritharadol, R., Srichana, T., 2017. Quantitative analysis of povidone-iodine thin films by X-ray photoelectron spectroscopy and their physicochemical properties. Acta Pharm. (Zagreb, Croatia) 67, 169–186.

Satoh, Y., Imai, S., 2020. Evaluation of dissolution flux of iodine from brackish lake sediments under different temperature and oxygenic conditions. Sci. Total Environ. 707, 135920.

Shih, C.-M., Wu, Y.-L., Wang, Y.-C., Kumar, S.R., Tung, Y.-L., Yang, C.-C., Lue, S.J., 2018. Ionic transport and interfacial interaction of iodide/iodine redox mechanism in agarose electrolyte containing colloidal titanium dioxide nanoparticles. J. Photochem. Photobiol., A 356, 565–572.

Shirai, T., Shimizu, T., Ohtani, K., Zen, Y., Takaya, M., Tsuchiya, H., 2011. Antibacterial iodine-supported titanium implants. Acta Biomater. 7, 1928–1933.

Shirai, T., Watanabe, K., Matsubara, H., Nomura, I., Fujiwara, H., Arai, Y., Ikoma, K., Terauchi, R., Kubo, T., Tsuchiya, H., 2014. Prevention of pin tract infection with iodine-supported titanium pins. J. Orthop. Sci. 19, 598–602.

Sulka, G.D., Kapusta-Kołodziej, J., Brzózka, A., Jaskuła, M., 2013. Anodic growth of TiO2 nanopore arrays at various temperatures. Electrochim. Acta 104, 526–535.

Teng, W., Zhang, Z., Wang, Y., Ye, Y., Yinwang, E., Liu, A., Zhou, X., Xu, J., Zhou, C., Sun, H., Wang, F., Zhang, L., Cheng, C., Lin, P., Wu, Y., Gou, Z., Yu, X., Ye, Z., 2021. Iodine immobilized metal–organic framework for NIR-triggered antibacterial therapy on orthopedic implants. Small 17, 2102315.

Tsuchiya, H., Shirai, T., Nishida, H., Murakami, H., Kabata, T., Yamamoto, N., Watanabe, K., Nakase, J., 2012. Innovative antimicrobial coating of titanium implants with iodine. J. Orthop. Sci. 17, 595–604.

Tverdokhlebov, S.I., Bolbasov, E.N., Shesterikov, E.V., Malchikhina, A.I., Novikov, V.A., Anissimov, Y.G., 2012. Research of the surface properties of the thermoplastic copolymer of vinilidene fluoride and tetrafluoroethylene modified with radio-frequency magnetron sputtering for medical application. Appl. Surf. Sci. 263, 187–194.

Ueoka, K., Kajino, Y., Kabata, T., Inoue, D., Yoshitani, J., Ueno, T., Yamamuro, Y., Shirai, T., Tsuchiya, H., 2020. The feasibility of iodine-supported processing for titanium with different surfaces. J. Orthop. Sci. 25, 1095–1100.

Valko, M., Morris, H., Cronin, M.T., 2005. Metals, toxicity and oxidative stress. Curr. Med. Chem. 12, 1161–1208.

Vielgut, I., Sadoghi, P., Wolf, M., Holzer, L., Leithner, A., Schwantzer, G., Poolman, R., Frankl, B., Glehr, M., 2015. Two-stage revision of prosthetic hip joint infections using antibiotic-loaded cement spacers: when is the best time to perform the second stage? Int. Orthop. 39, 1731–1736.

Wang, Y., Zhao, S., Li, G., Zhang, S., Zhao, R., Dong, A., Zhang, R., 2020. Preparation and in vitro antibacterial properties of anodic coatings co-doped with Cu, Zn, and P on a Ti–6Al–4V alloy. Mater. Chem. Phys. 241, 122360.

Wolcott, R.D., Cook, R.G., Johnson, E., Jones, C.E., Kennedy, J.P., Simman, R., Woo, K., Weir, D., Schultz, G., Hermans, M.H., 2020. A review of iodine-based compounds, with a focus on biofilms: results of an expert panel. J. Wound Care 29, S38–S43.

Wu, H., Zhang, X., Geng, Z., Yin, Y., Hang, R., Huang, X., Yao, X., Tang, B., 2014. Preparation, antibacterial effects and corrosion resistant of porous Cu–TiO2 coatings. Appl. Surf. Sci. 308, 43–49.

Xie, M., Zhong, Y., Wang, S., Tian, L., Wang, X., Hu, Y., Zeng, R., 2022. EGCG/Zn coating on titanium implants by one-step hydrothermal method for improving anticorrosion, antibacterial and osteogenesis properties. Mater. Chem. Phys. 292, 126872.

Yamaguchi, S., Le, P.T.M., Shintani, S.A., Takadama, H., Ito, M., Ferraris, S., Spriano, S., 2021. Iodine-loaded calcium titanate for bone repair with sustainable antibacterial activity prepared by solution and heat treatment. Nanomaterials-Basel 11, 2199.

Zhang, K., Zhang, B., Huang, C., Gao, S., Li, B., Cao, R., Cheng, J., Li, R., Yu, Z., Xie, X., 2019. Biocompatibility and antibacterial properties of pure titanium surfaces coated with yttrium-doped hydroxyapatite. J. Mech. Behav. Biomed. 100, 103363.